

## Solar light trapping in slanted conical-pore photonic crystals: Beyond statistical ray trapping

Sergey Eyderman, Sajeev John, and Alexei Deinega

Citation: *J. Appl. Phys.* **113**, 154315 (2013); doi: 10.1063/1.4802442

View online: <http://dx.doi.org/10.1063/1.4802442>

View Table of Contents: <http://jap.aip.org/resource/1/JAPIAU/v113/i15>

Published by the [American Institute of Physics](#).

---

### Additional information on J. Appl. Phys.

Journal Homepage: <http://jap.aip.org/>

Journal Information: [http://jap.aip.org/about/about\\_the\\_journal](http://jap.aip.org/about/about_the_journal)

Top downloads: [http://jap.aip.org/features/most\\_downloaded](http://jap.aip.org/features/most_downloaded)

Information for Authors: <http://jap.aip.org/authors>

## ADVERTISEMENT



**AIP Advances**

Now Indexed in Thomson Reuters Databases

Explore AIP's open access journal:

- Rapid publication
- Article-level metrics
- Post-publication rating and commenting

# Solar light trapping in slanted conical-pore photonic crystals: Beyond statistical ray trapping

Sergey Eyderman,<sup>a)</sup> Sajeev John, and Alexei Deinega

*Department of Physics, University of Toronto, 60 St. George Street, Toronto, Ontario M5S 1A7, Canada*

(Received 8 October 2012; accepted 3 April 2013; published online 19 April 2013)

We demonstrate that with only  $1\ \mu\text{m}$ , equivalent bulk thickness, of crystalline silicon, sculpted into the form of a slanted conical-pore photonic crystal and placed on a silver back-reflector, it is possible to attain a maximum achievable photocurrent density (MAPD) of  $35.5\ \text{mA}/\text{cm}^2$  from impinging sunlight. This corresponds to absorbing roughly 85% of all available sunlight in the wavelength range of 300–1100 nm and exceeds the limits suggested by previous “statistical ray trapping” arguments. Given the AM 1.5 solar spectrum and the intrinsic absorption characteristics of silicon, the optimum carrier generation occurs for a photonic crystal square lattice constant of 850 nm and slightly overlapping inverted cones with upper (base) radius of 500 nm. This provides a graded refractive index profile with good anti-reflection behavior. Light trapping is enhanced by tilting each inverted cone such that one side of each cone is tangent to the plane defining the side of the elementary cell. When the solar cell is packaged with silica (each pore filled with  $\text{SiO}_2$ ), the MAPD in the wavelength range of 400–1100 nm becomes  $32.6\ \text{mA}/\text{cm}^2$  still higher than the Lambertian  $4n^2$  benchmark of  $31.2\ \text{mA}/\text{cm}^2$ . In the near infrared regime from 800 to 1100 nm, our structure traps and absorbs light within slow group velocity modes, which propagate nearly parallel to the solar cell interface and exhibit localized high intensity vortex-like flow in the Poynting vector-field. In this near infrared range, our partial MAPD is  $10.9\ \text{mA}/\text{cm}^2$  compared to a partial MAPD of  $7\ \text{mA}/\text{cm}^2$  based on “ $4n^2$  statistical ray trapping.” These results suggest silicon solar cell efficiencies exceeding 20% with just  $1\ \mu\text{m}$  of silicon. © 2013 AIP Publishing LLC [<http://dx.doi.org/10.1063/1.4802442>]

## I. INTRODUCTION

One of the most important and limitless sources of energy for human consumption comes from sunlight. With the exception of nuclear energy, nearly all other sources of power in use today are derivatives of solar power in one way or another. Photovoltaic technology is a direct way to capture and harvest solar energy in real-time. To achieve high solar power conversion efficiency, one needs to use advanced materials in which sunlight is almost completely absorbed over a broad wavelength range, a broad range of incident angles, and in which photogenerated charge carriers need to travel only a short distance before being collected. Silicon is the most abundant and reliable material for solar energy harvesting. However, the intrinsic absorption length for light in crystalline silicon ranges from tens of nanometers in the blue (400 nm) range to tens of centimeters in the near infrared (800–1100 nm) at photon energy below the direct electronic band gap of silicon, but above the indirect gap. Despite weak intrinsic absorption in the red to near-infrared regime, it may be possible to absorb over 90% of available sunlight in the 400–1100 nm range in thick silicon slabs (100–300  $\mu\text{m}$ ) using classical ray trapping concepts. However, for charge carriers generated in such thick slabs to diffuse, separate across a p-n junction and be collected by electrodes prior to recombination losses, it is necessary to use very high quality crystalline silicon. This involves relatively high cost in the

production of solar cells. On the other hand, in thin film silicon structures ( $\leq 1\ \mu\text{m}$ ), the carrier diffusion length requirements are less stringent. The challenge remains to trap and absorb the maximum fraction of available incoming sunlight in a thin silicon film.

Most commercial solar cells now are made from wafers typically with a thickness of a few hundred microns of very pure crystalline or polycrystalline silicon. Silicon wafers are relatively expensive—about 40% of the final module cost. Therefore, there is a strong interest in designing solar cells based on thin films<sup>1–3</sup> with an equivalent active layer thickness of about  $1\ \mu\text{m}$ , with substantial reduction in the cost of energy production. However, this requires optimization of their light trapping<sup>4,5</sup> and antireflective capabilities<sup>6–13</sup> to obtain power conversion efficiencies comparable to thick silicon wafers. Moreover, light trapping in thin-films offers opportunities to surpass the performance of conventional thick solar cells through more effective carrier collection and nonlinear solar spectrum reshaping effects (up-conversion<sup>14</sup> and down-conversion<sup>15,16</sup>) enabled by strong light concentration effects. In this regard, the concepts of light localization<sup>17</sup> and photonic crystals (PCs)<sup>18–20</sup> provide a unique opportunity for light management in third generation solar cells.<sup>21,22</sup>

Solar cells consisting of thin film photonic crystals have been recently discussed in the literature. These include 1D,<sup>23,24</sup> 2D,<sup>25,26</sup> and 3D (Refs. 27–29) periodically structured matter. One practical 2D photonic crystal architecture consists of a periodic array of nanowires.<sup>30–33</sup> Silicon nanowire photonic crystals exhibit some light trapping effects

<sup>a)</sup>Author to whom correspondence should be addressed. Electronic mail: [eyderman@kintechlab.com](mailto:eyderman@kintechlab.com)

caused by multiple scattering. Another advantage of nanowires comes from the use of a radial P-N junction geometry. This leads to rapid separation of electrons and holes throughout the active, light-absorbing region, thereby reducing recombination losses. However, straight cylindrical nanowires are not optimized for either light-trapping or anti-reflection behavior.<sup>34,35</sup>

A traditional way to minimize reflection from a thick silicon solar cell is to texture the surface with pyramids or cones.<sup>6-13</sup> In the long wavelengths limit, the textured coating behaves like a graded index film. Choosing special graded index profiles in the form of polynomial or exponential shape functions<sup>6</sup> allows control of the rate of the reflectance. In the short wavelength limit, reduced reflection can be understood using geometrical ray optics.<sup>6,12,13</sup> It was shown that ideal square pyramids (with no gaps between pyramid bases) exhibit exponential decrease in reflection with height.<sup>6</sup> Antireflective properties of textured coatings have been also investigated for a wide range of size-to-wavelengths ratios by direct numerical solution of Maxwell's equations and compared with results obtained by effective medium theory and ray tracing in the long- and short-wave limits, respectively.<sup>6</sup> In the visible range, optimal anti-reflection is achieved when the lateral size of each pyramid and texture period is of the order of the wavelength.

While optimal anti-reflection at the top surface of a solar cell is crucial to its performance, light trapping below the surface is important for those wavelength where the intrinsic absorption length scale is long compared to the film thickness. In the geometrical ray optics limit, it was suggested<sup>36,37</sup> that significant light trapping could be achieved by total internal reflection, if incoming light rays are scattered at an oblique angle by the top surface. Such rays would have a long dwell time (long path length) within the film and be absorbed. In this ray optics picture, a statistical ray trapping and absorption "limit" was postulated<sup>36</sup> using various questionable assumptions. Given the fact that these assumptions do not apply to microstructures such as photonic crystals, we argue that no such limit in fact exists. Instead, we will refer to this "limit" as a benchmark. The first of these assumptions is that top surface of the cell possess perfect anti-reflection behavior at all wavelengths of incoming light. The second assumption is that the top surface (taken to be randomly textured) scatters light in a statistically random direction (with a probability density proportional to the cosine of the angle relative to normal) throughout the lower hemisphere of possible wave vectors, for all wavelengths, of incoming light. The third assumption is that the top surface of the solar cell (taken previously to be randomly textured and perfectly anti-reflecting to incoming light) can at the same time provide perfect total internal reflection for all internal light rays beyond a fixed critical angle and perfect escape of light within the critical angle. Although no real material surface can satisfy these assumptions, even in principle, the statistical ray trapping arguments has provided a valuable benchmark for absorption of light in textured solar cells designs. A more detailed discussion of this benchmark is given in Sec. IV below.

Violations of the assumptions underlying the statistical ray trapping limit are particularly pronounced in microstructures with features (or overall thickness) comparable to the wavelength of light. For example, it has been demonstrated that certain PCs exhibit the phenomenon of parallel-to-interface refraction (PIR).<sup>38</sup> Here, light from a broad range of incident angles is refracted into small set of oblique angles, nearly parallel to the air-PC interface. This is distinct from the statistical ray trapping assumption that refracted rays are distributed over the lower hemisphere of possible wave vectors with a Lambertian<sup>39</sup> probability. In a semi-infinite PC, the PIR effect is accompanied by an enhanced electromagnetic density of states. In a finite thickness PC film, this is manifested in a large density of high quality factor optical resonances. It was shown<sup>38</sup> that when the resonant optical cavity dwell time is matched to the intrinsic absorption time of the underlying material, 100% of the incoming light at the specific frequency of the resonance could be absorbed. This leads to absorption beyond the statistical ray trapping limit at specific wavelengths.

Despite the advantages of photonic crystal based light trapping relative to simple statistical ray trapping (by total internal reflection), it has not previously been demonstrated that absorption in a photonic crystal thin film could exceed the benchmark suggested by statistical ray trapping, when integrated over the entire solar spectrum, using the same amount of silicon. The statistical ray trapping limit has only been surpassed previously in narrower frequency windows.<sup>40</sup> In a recent, modulated silicon nano-wire design<sup>34</sup> (that facilitates both photonic crystal light-trapping and graded-index anti-reflection), strong optical cavity resonances enabled absorption beyond the statistical ray trapping limit at numerous wavelength in the red to near infrared regime. However, the integrated absorption over the entire wavelength range from 400 to 1000 nm fell short of the absorption limit from statistical ray trapping. Using 1  $\mu\text{m}$  in equivalent bulk thickness of silicon, the modulated silicon nanowire PC in a  $\text{SiO}_2$  background, exhibited a maximum achievable photo-current density (MAPD) of  $27.17 \text{ mA/cm}^2$  in the range of 400–1100 nm.<sup>34</sup> This is slightly below the hypothetical ray trapping benchmark of  $31.2 \text{ mA/cm}^2$ . On the other hand, using modulated radial P-N junction and appropriate choice of contacts position, one can achieve 15% power conversion efficiency for modulated Si nanowires.<sup>35</sup>

In this paper, we present a silicon photonic crystal architecture that traps and absorbs light over the entire solar spectrum in excess of hypothetical statistical ray trapping benchmark. Our architecture, consisting of a square lattice of slanted conical nanopores in Si filled with  $\text{SiO}_2$ , combines the effects of graded index anti-reflection and photonic crystal light trapping. With only 1  $\mu\text{m}$  (equivalent bulk thickness) of crystalline silicon and a silver back-reflector, our PC provides a MAPD of  $35.5 \text{ mA/cm}^2$  without  $\text{SiO}_2$  packaging and MAPD of  $33.8 \text{ mA/cm}^2$  with  $\text{SiO}_2$  packaging. Both values exceed the Lambertian<sup>36</sup> statistical ray trapping benchmark MAPD of  $32.6 \text{ mA/cm}^2$  over the integrated wavelength range of 300–1100 nm. Our structure provides a potential 25% improvement in the power conversion efficiency of the best available tapered/modulated nanowire designs.<sup>35</sup> This

suggests power efficiencies in the range of 20% may be possible for single-junction silicon solar cells using only  $1\ \mu\text{m}$  of crystalline silicon.

In Sec. II, we describe our method of calculation. In Sec. III, we compare the MAPD of cylindrical pore, straight conical pore, and slanted conical pore photonic crystal geometries. In Sec. IV, we demonstrate that our slanted conical pore PC surpasses previously proposed statistical ray trapping limits. In Sec. V, we demonstrate the good angular response of our architecture for light incident from off-normal directions. In Sec. VI, we make concluding remarks.

## II. METHOD OF SIMULATION

Numerical simulations were performed using the finite-difference time-domain (FDTD) method<sup>41</sup> with the help of the Electromagnetic Template Library.<sup>42</sup> We use a standard scheme of the FDTD calculation in which propagation of a wave impulse through the structure is modeled. During the numerical experiment, the amplitudes of the reflected and transmitted waves were recorded, transformed to the frequency domain, and normalized by the incident spectrum. In this way, we obtain directly the transmission  $T(\omega)$ , reflection  $R(\omega)$ , and indirectly the absorption  $A(\omega) = 1 - T(\omega) - R(\omega)$  coefficients for given light frequency  $\omega$ , incident angle, and polarization. The absorption coefficient was also independently and directly evaluated using the formula:

$$A = \frac{\int \omega \epsilon_0 \text{Im}(\epsilon) |E|^2 dx dy dz}{\int \text{Re}[E_0 \times H_0^*] \cdot \mathbf{n} dx dy}. \quad (1)$$

Here,  $\omega$  is an angular frequency,  $E$  is the electric field amplitude calculated at each point of a computational grid located within silicon,  $\epsilon$  is the frequency-dependent and complex dielectric permittivity of silicon,  $E_0$  and  $H_0$  are electric and magnetic vectors of the incident plane wave,  $\mathbf{n}$  is a normal unit vector, and the superscript \* indicates the complex conjugate. Both the direct and indirect methods for calculating the absorption give identical results.

The MAPD, in which all generated carriers are assumed to be collected, is calculated by integrating the simulated absorption with incident solar Air Mass 1.5 Global Spectrum<sup>43</sup> intensity  $I(\lambda)$  over the required wavelength range. Assuming that each absorbed photon translates into a single electron-hole pair that is separated across a P-N junction and collected without recombination losses, we obtain the maximum achievable short circuit current for AM 1.5 solar spectrum in the spectral window  $[\lambda_{\min}, \lambda_{\max}]$ , all collimated into normal incidence

$$J_{\lambda_{\min}}^{\lambda_{\max}} = \int_{\lambda_{\min}}^{\lambda_{\max}} \frac{e\lambda}{hc} I(\lambda) A(\lambda) d\lambda. \quad (2)$$

Here,  $I(\lambda)$  is the incident AM 1.5 light intensity,  $A(\lambda)$  is the absorption coefficient obtained according to Eq. (1),  $h$  is Planck's constant,  $e$  is the electronic charge, and  $c$  is the speed of light.

We use a subpixel smoothing technique<sup>44</sup> to eliminate any staircase effect caused by rectangular FDTD mesh. This

technique significantly improves FDTD accuracy for arbitrary shaped structures. To reduce numerical reflection from the artificial absorbing perfectly matched layers (PMLs),<sup>41</sup> additional back absorbing layers technique is used.<sup>45</sup> We also consider the AM 1.5 solar spectrum collimated at off-normal incidence. Oblique incidence of a plane wave on the structure is modeled by the iterative FDTD algorithm.<sup>46,47</sup>

The experimental data on the silicon dielectric permittivity is taken from Ref. 48. The frequency dependence  $\epsilon(\omega)$  is assigned in FDTD by considering a modified Lorentz model where dielectric polarization depends both on the electric field and its first time derivative.<sup>49</sup> This model provides an accurate fit of the optical response of bulk crystalline silicon to sunlight over the wavelength range from 300 to 1100 nm, while conventional Debye, Drude, and Lorentz approximations fail. Fitting of silicon dielectric function is found with the help of open MATLAB program.<sup>50</sup>

## III. MAXIMAL SHORT-CIRCUIT CURRENT CALCULATION

The MAPD is an alternative measure of the total amount of AM 1.5 sunlight absorbed in a given structure. For 100% absorption of sunlight in the range of 400–1100 nm, the MAPD corresponds to  $42.1\ \text{mA}/\text{cm}^2$ . For ranges of 350–1000 nm and 300–1100 nm, the MAPD is  $43.1\ \text{mA}/\text{cm}^2$  and  $43.5\ \text{mA}/\text{cm}^2$ , respectively.

For calibration purposes, we begin the optimization process for the short circuit current of solar cells from the absorption characteristics of a free-standing bulk silicon slab with the thickness of  $1\ \mu\text{m}$ . Calculating the absorption coefficient and using formula (2) in the spectral range of 400–1100 nm, we obtain the MAPD of  $J = 7.9\ \text{mA}/\text{cm}^2$ . In other words, less than 20% of the AM 1.5 sunlight in the 400–1100 nm is absorbed. The overall absorption spectrum at normal incidence, exhibiting a number of Fabry-Perot resonances, is shown in Fig. 1.

This simple solar cell architecture lacks adequate light trapping and antireflective properties. The majority of the incident light is transmitted or reflected rather than absorbed. Consequently, only a maximum of 60% of sunlight at a

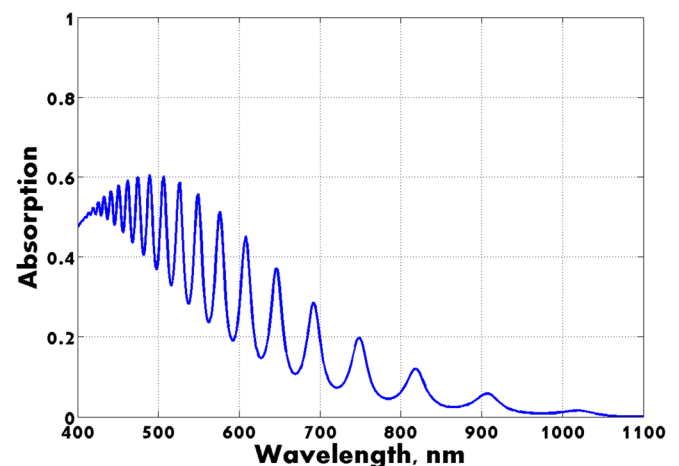


FIG. 1. Absorption spectrum for free standing bulk silicon thin film with thickness of  $1\ \mu\text{m}$  with no metallic back-reflector.

wavelength near 500 nm is absorbed and a dramatic drop in absorption occurs for all wavelengths longer than 700 nm. As discussed earlier, a number of micro- and nano-structured geometries have been proposed to increase absorption.

In the present paper, we focus our attention on inverted structures consisting of a periodic array of holes in bulk silicon. We suggest that conical pores are highly advantageous since they provide an effective graded average refractive index to incoming sunlight and therefore exhibit stronger antireflective properties in comparison with their straight counterparts. However, for calibration, we first consider light impinging (at normal incidence) on a square lattice of cylindrical holes in bulk silicon filled with glass (refractive index  $n = 1.45$ ). The optimization process is as follows: for a given geometry, we calculate (using FDTD) the absorption spectrum for different radii and lattice constants to determine the maximal short circuit current defined by Eq. (3). The result in the case of an equivalent bulk thickness of crystalline silicon of  $1.5 \mu\text{m}$  is shown in Fig. 2. Here, the photonic crystal slab rests on a semi-infinite glass substrate with no metallic back-reflector. The maximal short circuit current obtained is  $J = 19.5 \text{ mA/cm}^2$  for the optimized choice of lattice constant  $a = 550 \text{ nm}$  and cylinder radius  $r = 200 \text{ nm}$ . It is interesting to note here that the MAPD obtained for optimized cylindrical nano-pores is slightly less than the corresponding MAPD for cylindrical nano-wires. It was demonstrated earlier<sup>34</sup> that with only  $1 \mu\text{m}$  of silicon sculpted into the form of a square lattice photonic crystal with  $a = 350 \text{ nm}$  and  $r = 80 \text{ nm}$  (embedded in a glass background and sitting on a glass substrate) that the MAPD reaches  $20.7 \text{ mA/cm}^2$ . This advantage of nano-wires over nano-cones is lost, however, when vertical shape modulation of the pores/wires are introduced.

The optimization made for the same parameters with air filling of cylindrical holes gives a MAPD of  $J = 22.3 \text{ mA/cm}^2$  due to reduced reflection and better coupling of the incident

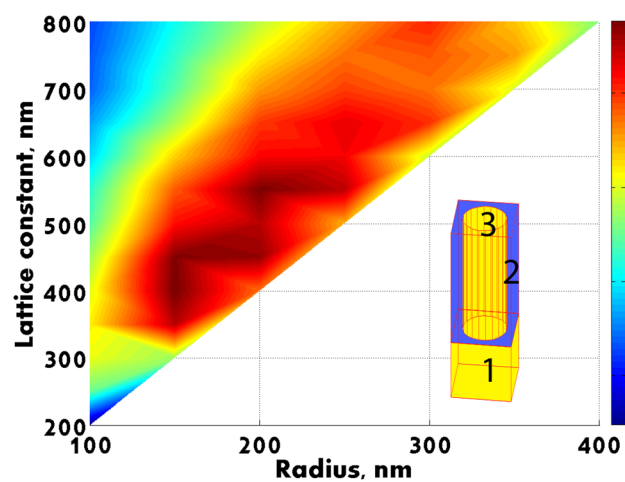


FIG. 2. Short circuit current optimization (normal incidence of AM 1.5 sunlight) for vertical cylindrical holes in bulk silicon arranged in a square lattice and filled with glass with the refractive index  $n = 1.45$  and deposited on infinite glass substrate. The optimal parameters are  $r = 200 \text{ nm}$ ,  $a = 550 \text{ nm}$ , for an equivalent bulk thickness of silicon  $1.5 \mu\text{m}$ . The color bar on the right indicates MAPD in units of  $\text{mA/cm}^2$ . Maximal short circuit current obtained is  $J = 19.5 \text{ mA/cm}^2$  in the spectral range of 400–1100 nm. The elementary cell of the structure is shown in the inset. Regions 1, 2, and 3 indicate infinite glass substrate, silicon, and cylinder filled with glass, respectively.

light to waveguide modes of the 2D photonic crystal slab. A closely related 3D PC geometry consists of two slanted cylindrical pores filled with glass in each unit cell criss-crossing at  $90^\circ$  to form a simple-cubic silicon woodpile structure. We obtained a MAPD of  $J = 20.5 \text{ mA/cm}^2$ , providing only a small improvement relative to vertical pores. More sophisticated geometries based on several cylindrical pores in an elementary cell and various angles between pores did not yield substantial improvement to the absorption coefficient.

Architectures based on cylindrical straight holes suffer from significant reflection losses. Anti-reflection behavior requires a smooth gradient of the dielectric permeability in the direction of light propagation. This graded index can be realized using conical rather than straight pore arrays. We show below that by using suitable conical pore silicon photonic crystals, with an equivalent bulk thickness of only  $1 \mu\text{m}$ , it is possible to trap and absorb more sunlight than in the thicker ( $1.5 \mu\text{m}$ ) cylindrical pore photonic crystals discussed above.

In Fig. 3, we present a map for MAPD optimization using an array of conical (vertical) holes in bulk silicon arranged in a square lattice. Sunlight is assumed collimated at normal incidence and the silicon pores are filled with glass ( $n = 1.45$ ). This structure is assumed to sit on semi-infinite silica substrate with no back-reflector. Maximal short circuit current obtained is  $J = 24.1 \text{ mA/cm}^2$ , using only  $1 \mu\text{m}$  of silicon. This is 20% more than in the optimized design with cylindrical pores, using  $1.5 \mu\text{m}$  of silicon.

The most remarkable structure considered in this paper is a photonic crystal consisting of slanted conical pores. In Fig. 4, we present a map of MAPD optimization.

Maximal short circuit current obtained for the structure depicted on the inset of Fig. 4 is  $J = 25.7 \text{ mA/cm}^2$ . This is 6% better than the structure with vertical pores due to the

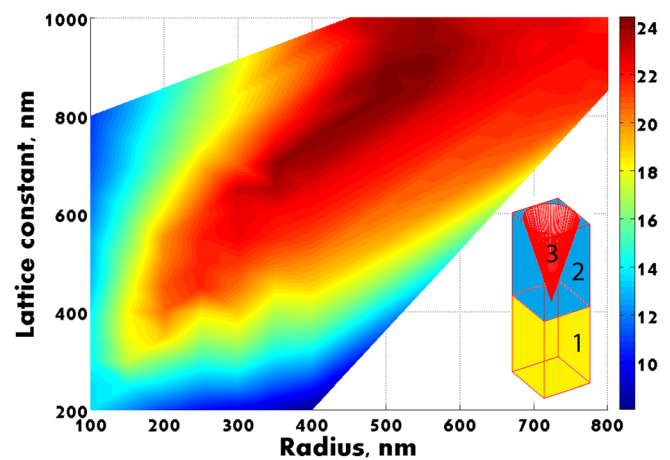


FIG. 3. Short circuit current optimization (normal incidence of AM 1.5 sunlight) for vertical conical holes in bulk silicon arranged in a square lattice and filled with glass with the refractive index  $n = 1.45$ . The photonic crystal slab rests on an infinite glass substrate. For an equivalent bulk thickness of silicon  $1.0 \mu\text{m}$ , optimal parameters are  $r = 500 \text{ nm}$ ,  $a = 800 \text{ nm}$ . The color bar on the right indicates MAPD in units of  $\text{mA/cm}^2$ . Maximal short circuit current obtained is  $J = 24.1 \text{ mA/cm}^2$  in the spectral range of 400–1100 nm. The design is highly robust and nearly the same MAPD is possible in a range of parameters  $300 \text{ nm} < r < 600 \text{ nm}$  and  $600 \text{ nm} < a < 1000 \text{ nm}$ . The elementary cell of the structure is shown in the inset. Regions 1, 2, and 3 indicate infinite glass substrate, silicon, and cone filled with glass, respectively.

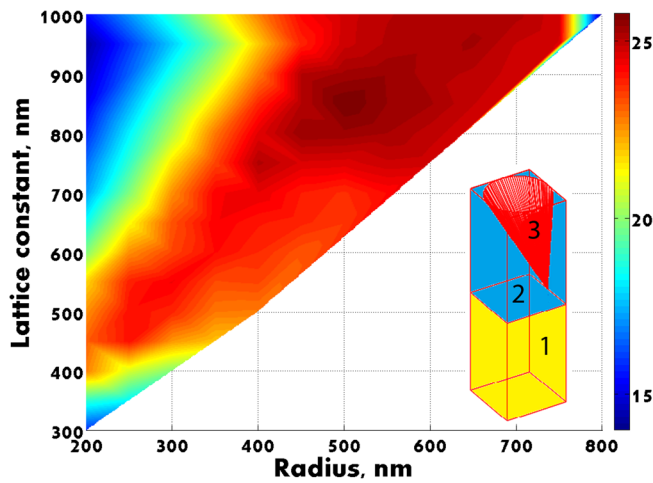


FIG. 4. Short circuit current optimization (collimated AM 1.5 sunlight at normal incidence) for slanted conical holes in bulk silicon arranged in a square lattice and filled with glass with the refractive index  $n = 1.45$ . The photonic crystal slab rests on an infinite glass substrate. For an equivalent bulk thickness of silicon of  $1.0 \mu\text{m}$ , optimal parameters are  $r = 500 \text{ nm}$ ,  $a = 850 \text{ nm}$ . The color bar on the right indicates MAPD in units of  $\text{mA}/\text{cm}^2$ . Maximal short circuit current obtained  $J = 25.7 \text{ mA}/\text{cm}^2$  in the spectral range of  $400\text{--}1100 \text{ nm}$ . The elementary cell of the structure is shown in the inset. Regions 1, 2, and 3 indicate infinite glass substrate, silicon, and cone filled with glass, respectively.

stronger antireflection properties. This interpretation is supported by the reflection coefficients obtained for a related geometry. We consider two structures consisting of air cones in a semi-infinite substrate, one with vertical cones and the other with slanted cones. In order to exclude the influence of absorption influence and light trapping, we consider a hypothetical substrate material with a purely real refractive index  $n = 3.5$  and no absorption. The comparison of reflection is presented in Fig. 5.

Fig. 5 depicts that slanted conical pores in bulk (non-absorbing) silicon exhibits strong antireflective properties causing less than 3.5% reflection throughout the relevant solar spectrum. Therefore, slanted cones are preferable to their vertical counterpart. We also studied the sensitivity of this structure to geometrical variations. We found that for

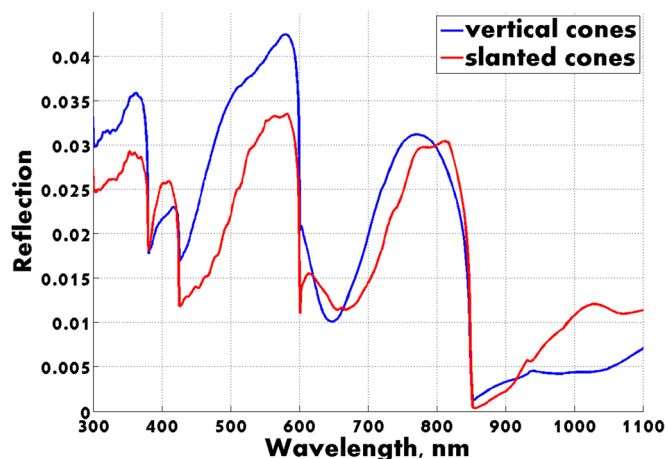


FIG. 5. Reflection coefficient comparison for slanted and vertical conical air pores in a hypothetical semi-finite substrate material with refractive index  $n = 3.5$  and no absorption. All geometrical parameters are the same as in Figs. 3 and 4:  $r = 500 \text{ nm}$ ,  $a = 850 \text{ nm}$ .

non-overlapping conical pores with  $r = 425 \text{ nm}$  and  $a = 850 \text{ nm}$  the MAPD is slightly reduced to  $J = 24.5 \text{ mA}/\text{cm}^2$ . In addition, it was shown that fabrication errors of  $\pm 50 \text{ nm}$  in radius or lattice constant do not substantially degrade the anti-reflective behavior.

The overall light absorption in our slanted conical nanopore photonic crystal, without any back-reflector, is very similar in magnitude to previously studied modulated silicon nanowire photonic crystal.<sup>34</sup> A strong radial modulation near the bottom of nanowires provided strong back-reflection of near-infrared light. For those nanowires, the addition of a metallic reflector provided only a small improvement in overall light absorption. The situation is very different for our conical nano-pore PC, where substantial transmission of long wavelength light occurs into the  $\text{SiO}_2$  substrate below. Unlike the case of nanowires, a substantial improvement in the MAPD is realized by including a metallic back-reflector to the conical nano-pore photonic crystal.

By adding a back-reflector made of some low-loss material such as silver at the bottom of our conical nano-pore array, transmission through the structure is eliminated and only leakage of light from the top surface needs to be addressed. The thickness of the backreflector should be larger than a skin depth of the relevant metal. Accordingly, we choose the back-reflector to be  $100 \text{ nm}$  thick. The physical explanation of the absorption enhancement in the presence of a back-reflector is the stronger coupling of incident light to parallel-to-interface waveguide modes formed by the nano-cones array. Our light trapping scheme relies on the ability of this structure to diffract/refract incident light into slow group velocity modes that travel nearly parallel to the silicon air interface. The silver back-reflector couples light (that would otherwise be transmitted) into these modes as well.

In order to elucidate the nature of light trapping in the wavelength range of  $850\text{--}1100 \text{ nm}$ , we calculate energy density and Poynting vector distribution in our structure. First, in Fig. 6, we present an absorption spectrum for a free-standing, silicon slanted nano-cone array filled with air. To make the picture more clear and energy flow more pronounced, we also remove the back reflector, thereby avoiding multiple reflections at the bottom of our silicon photonic crystal.

Absorption peaks in Fig. 6 in the wavelength range of  $1000\text{--}1100 \text{ nm}$  are attributed to strong light trapping since the intrinsic absorption of silicon is very weak. We focus on the absorption peak marked with arrow 1 (corresponding to the wavelength  $1027 \text{ nm}$ ). In Figs. 7 and 8, Poynting vectors and energy density distribution for this peak are plotted in projections onto two orthogonal planes. Fig. 7 corresponds to a slice passing through the center of the cone showing its asymmetric slant. Fig. 8 corresponds to a perpendicular slice (see the inset) again passing through the center of the cone, but showing a symmetric profile.

Figs. 7 and 8 reveal that the light trapping in our structure occurs through the energy flow parallel to the air-silicon interface but strongly augmented by circulation in certain areas. The energy density distribution shows high intensity peaks mostly concentrated in the silicon region where the

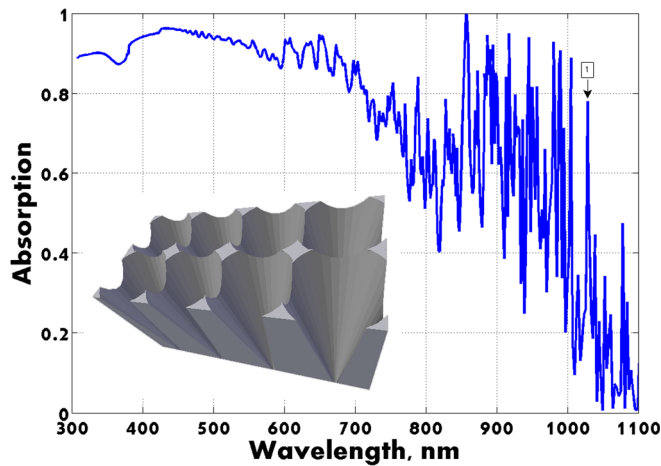


FIG. 6. Absorption coefficient for slanted conical air pores in a free-standing bulk silicon film (with air above and below). All geometrical parameters are same as in Figs. 3 and 4:  $r = 500$  nm,  $a = 850$  nm. A top view of the structure is shown in the inset. Since the cone diameter at the top slightly exceeds the lattice constant, the top surface appears as a lattice of small protrusions with a diamond-like cross-section.

Poynting vector exhibits vortex-like circulation patterns. This circulation enhances the dwell time of light in the thin-film. Similar slices at different wavelengths corresponding to minima in the absorption reveal an energy density that is less intense and more concentrated within the interior part of the cones.

In order to enhance deflection of sunlight into parallel-to-interface modes, we add a hemispherical modulation in the glass packaging on the top of solar cell (see the inset and parameters in Fig. 9). This modulation takes the form of a part of a sphere with a larger radius than the top of the  $\text{SiO}_2$  cone. The simulation of the maximum achievable short

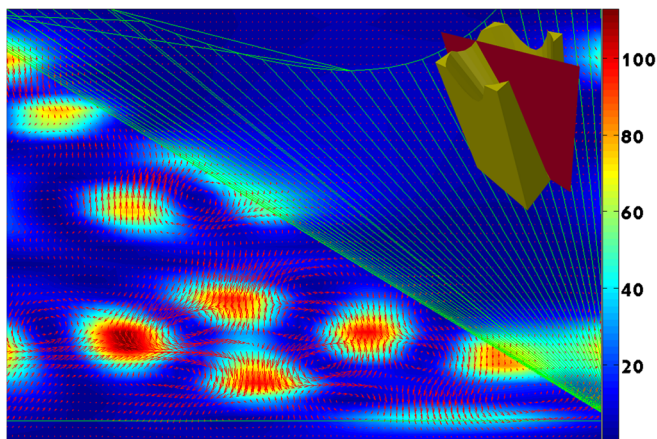


FIG. 7. Orthogonal slice for Poynting vector and the energy density distribution in a free-standing bulk silicon film for a resonance at wavelength of 1027 nm. Energy flow exhibits circulation between the high intensity regions (dark red) in addition to overall "parallel-to-interface flow." The inset indicates the computational domain (cutting slice) at the center in a plane of cone inclination. Green lines show the projection of the cone to this plane. All geometrical parameters are the same as in Fig. 4:  $r = 500$  nm,  $a = 850$  nm. The color bar on the right hand side indicates a ratio  $E_{2s}/E_{2w}$ , where  $E_s$  and  $E_w$  are electric fields in the structure and in the incoming plane wave, respectively. These fields are obtained during the numerical experiment and transformed to the frequency domain. A factor of more than 100 intensity enhancement is apparent in specific hot spots.

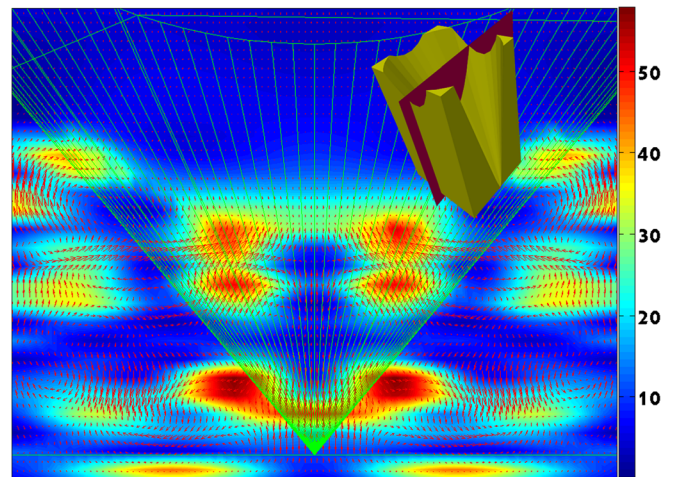


FIG. 8. Orthogonal slice for Poynting vector and the energy density distribution in a free-standing bulk silicon film for the wavelength of 1027 nm. Here, circulation patterns and high intensity peaks are concentrated in the silicon region. The inset indicates the computational domain (cutting slice) at the center in a plane perpendicular to the plane of cone inclination. Green lines show the projection of the cone to this plane. All geometrical parameters are the same as in Fig. 4:  $r = 500$  nm,  $a = 850$  nm. The color bar on the right hand side indicates a ratio  $E_{2s}/E_{2w}$ , where  $E_s$  and  $E_w$  are electric fields in the structure and in the incoming plane wave, respectively. These fields are obtained during the numerical experiment and transformed to the frequency domain.

circuit current in the spectral range of 400–1100 nm for a slanted nano-pore PC in bulk silicon with a perfect conducting reflector and modulated  $\text{SiO}_2$  packaging on the top gives the MAPD of  $J = 31.8$  mA/cm<sup>2</sup> for a flat top and  $J = 32.6$  mA/cm<sup>2</sup> in a presence of modulation. We confirmed these numbers by calculating the volume integral (1). The result is the same as the indirect absorption inferred from

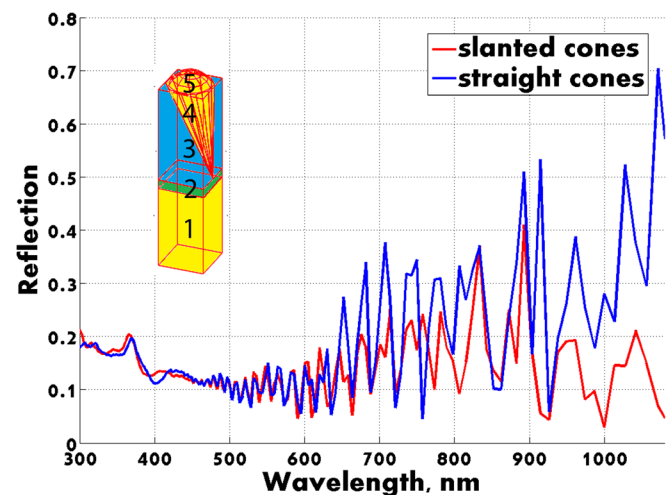


FIG. 9. Comparison of reflection coefficients obtained for vertical and slanted nano-cone arrays with a silver back-reflector (including small absorption losses in metal) and a glass modulation on the top. The elementary cell geometry corresponding to the slanted nano-cone array is depicted in the inset. The overall depth of nanopores is  $1.6$   $\mu\text{m}$ . Region 1—infinite glass substrate, 2—silver backreflector, 3—bulk silicon, 4—slanted cone filled with glass, 5—glass modulation on the top. The geometrical parameters are: lattice constant  $a = 850$  nm, cone top radius  $r = 500$  nm, equivalent bulk thickness of silicon  $w = 1$   $\mu\text{m}$ , period of modulation  $p = 850$  nm, height of  $\text{SiO}_2$  dome  $h = 200$  nm,  $\text{SiO}_2$  dome base radius  $r_1 = 500$  nm, thickness of silver back reflector  $b = 100$  nm.

reflection. When the perfect conductor is replaced by a realistic silver back-reflector, the MAPD of the fully packaged structure drops from 32.6 mA/cm<sup>2</sup> to 32.3 mA/cm<sup>2</sup> in the spectral range of 400–1100 nm.

In Fig. 9, we present a comparison of reflection obtained for vertical vs. slanted nano-cones arrays including a realistic silver back-reflector and a glass modulation on the top. We see that the slanted-cones array give a substantial reduction of a reflection coefficient in the spectral range of 800–1100 nm in comparison with its vertical counterpart.

The MAPD of  $J = 32.6 \text{ mA/cm}^2$  obtained for slanted conical nanopores filled with SiO<sub>2</sub> with a perfect conductor can be improved by removing the SiO<sub>2</sub> packaging and simply filling the nanocones with air and no texturing on the top. Since the majority of published literature quotes solar cell absorption characteristics without any SiO<sub>2</sub> packaging, we discuss how the performance of our architecture improves in the absence of packaging. However, such a packaging may be essential for passivation of electronic surface states and overall stability and reliability of the solar cell. Due to a better index-matching and improved anti-reflection, we obtain MAPD  $J = 34.2 \text{ mA/cm}^2$  in the spectral range of 400–1100 nm, and the MAPD  $J = 35.5 \text{ mA/cm}^2$  in the spectral range of 300–1100 nm.

**IV. COMPARISON TO STATISTICAL RAY TRAPPING**

In this section, we present a detailed comparison of our solution of Maxwell’s equations in the slanted conical nanopore photonic crystal with the statistical ray trapping benchmark for a solar cell with the same equivalent bulk thickness (1 μm) of silicon. Numerical results of this comparison are presented in Fig. 11. However, in order to clarify the nature of the ray trapping picture, we present a brief derivation of its content. In the ray trapping picture, the wave nature of light is ignored for the most part (except for the requirement of total internal reflection).

Consider a slab of solid material, with uniform refractive index  $n$ , of thickness  $L$ , placed on a perfectly reflecting flat mirror plane (Fig. 10(a)).

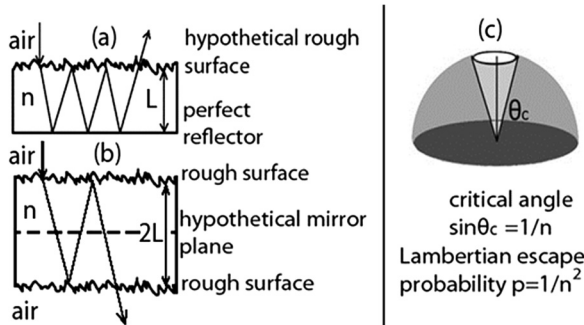


FIG. 10. (a)–(c) Geometry for statistical ray trapping: (a) A slab of solid material, with uniform refractive index  $n$ , of thickness  $L$ , placed on a perfectly reflecting flat mirror plane and hypothetical rough top surface with zero external reflection but “perfect” internal reflection, (b) the mathematically equivalent free-standing slab of thickness  $2L$  has both top and bottom surfaces with properties (i)–(iii) (see text), (c) the escape cone from total internal reflection. For a Lambertian internal probability distribution of light propagation, the escape probability  $p = 1/n^2$ .

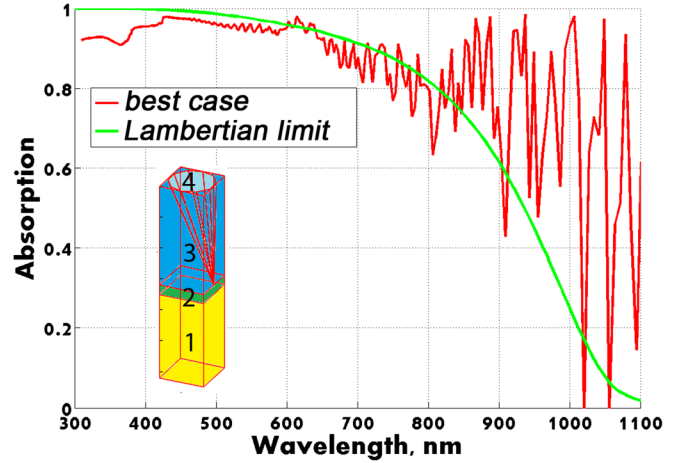


FIG. 11. Comparison of the absorption spectrum obtained for slanted conical nano-pores photonic crystal without SiO<sub>2</sub> packaging (see the inset) with the Lambertian statistical ray trapping limit (5). All geometrical parameters are the same as in Fig. 6. The elementary cell of the structure is shown in the inset. Regions 1, 2, 3, and 4 indicate infinite glass substrate, silver back-reflector, silicon, and cones filled with air, respectively.

The top surface of the slab is assumed to be rough and possess three remarkable hypothetical properties:

- (i) The surface causes no reflection of incoming light.
- (ii) The surface causes total internal reflection of light for light propagating at an angle (relative to the normal) greater than a critical angle  $\theta_c$  (where  $\sin\theta_c = 1/n$ ) but allows perfect escape of internal light at angles less than  $\theta_c$ .
- (iii) The surface is rough and causes both incident light and total internal reflected light to be randomly re-directed into an angle  $\theta$  with respect to the normal within the slab with a probability distribution  $g(\theta)$ .

In order to simplify the discussion we replace the above slab (with perfect mirror) with a mathematically equivalent free-standing slab of thickness  $2L$ . The equivalent free-standing slab (Fig. 10(b)) has both top and bottom surfaces with properties (i)–(iii).

When internal light (with unknown, random angle) impinges on a surface, it is assigned a probability,  $p$ , to escape the slab (into air). This probability is defined by the fraction of light within the solid angle of the escape cone (defined by the condition of total internal reflection) relative to the total light within the solid angle  $2\pi$  propagating toward the surface (Fig. 10(c))

$$p \equiv \int_0^{2\pi} d\varphi \int_0^{\theta_c} d\theta \sin\theta g(\theta). \tag{3}$$

In the case of so-called “Lambertian surface” [39], the normalized probability density is given by  $g(\theta) = \frac{1}{\pi} \cos\theta$ ,  $0 \leq \theta \leq \pi/2$ . In this case, an elementary integration of Eq. (3) yields the result that  $p = 1/n^2$ .

According to the assumed properties (ii) and (iii) it follows that light can make multiple “bounces” within the slab (of thickness  $2L$ ) before escaping. We define,  $m$ , to be the number traversals of light across the thickness  $2L$  and  $G(m)$  to be the probability that light will make precisely  $m$

traversals before escaping. Clearly  $G(1) = p$  since this is the condition that light escapes after just one traversal.  $G(m) = p(1 - p)^{m-1}$  since this is the condition that light does not escape in the first  $m - 1$  attempts but finally does escape on the  $m^{\text{th}}$  attempt. It is easy to verify that  $\sum_{m=1}^{\infty} G(m) = 1$ .

The average number of traversals of light across the slab is given by  $\langle m \rangle \equiv \sum_{m=1}^{\infty} mG(m) = 1/p$ . According to assumption (iii), upon each internal reflection, light is redirected into a random angle  $\theta$  and so each traversal corresponds to a path length of  $2L/\cos\theta$ . It follows that the average traversal length on a single pass (through the free-standing slab of thickness  $2L$ ) is given by

$$L_{\text{avg}} \equiv \int_0^{2\pi} d\varphi \int_0^{\pi/2} d\theta \sin\theta g(\theta) \frac{2L}{\cos\theta}. \quad (4)$$

Again, assuming Lambertian statistics,  $g(\theta) = \frac{1}{\pi} \cos\theta$ , the above integral reduces to  $L_{\text{avg}} = 4L$ . It follows that the overall characteristic path length for multiple internal reflections is given by  $L_{\text{trap}} = (2L)\langle m \rangle = 4n^2L$ . This is precisely the length scale alluded to in the previous literature<sup>46</sup> on statistical ray trapping and referred to as the Lambertian or “ $4n^2$  limit.”

We note, here, that the limit derived above is somewhat arbitrary. Any real surface will almost certainly violate aspects of assumptions (i) and (ii). More importantly, the photonic crystal surfaces that we consider violate the assumption of Lambertian probability density for light propagation within the slab. An important example is a photonic crystal exhibiting the phenomenon of PIR.<sup>34,38</sup> Here, the probability density  $g(\theta)$  is highly peaked in a direction closer to  $\pi/2$ . In the above analysis, this would greatly reduce the escape probability  $p$  and increase the average single pass traversal length  $L_{\text{avg}}$ . Moreover, Bragg scattering effects would cause multiple bounces of light even within a single traversal of the slab. Consequently, there is simply no “ $4n^2$  limit” in such a microstructured slab.

Given the characteristic trapping length scale  $L_{\text{trap}}$  for the non-absorbing medium, we can define the benchmark absorption coefficient for statistically trapped light when the slab is also endowed with characteristic absorption length  $l_{\text{abs}}$ . Following Ref. 52, the temporal rate of escape of light is given by  $v/L_{\text{trap}}$ , where  $v = c/n$  is the speed of light in the slab, and the temporal rate of absorption is  $v/L_{\text{abs}}$ . Since light must either be absorbed in the slab or escape the slab, it follows that the probability of absorption,  $A$ , is the ratio of the absorption rate to the rate of both absorption and escape combined:  $A = (1/L_{\text{abs}})/(1/L_{\text{abs}} + 1/L_{\text{trap}})$ . The probability of absorption can be identified with the fraction of incident light that is actually absorbed. Introducing the intrinsic absorption coefficient  $\alpha \equiv 1/L_{\text{abs}}$  of the material, it follows that

$$A = 1 - \frac{1}{1 + \alpha L_{\text{trap}}}. \quad (5)$$

We obtain the benchmark absorption profile discussed earlier<sup>52</sup> by setting  $L_{\text{trap}} = 4n^2L$ . Here  $n = 3.5$  is the real part of refractive index of silicon,  $\alpha = 4\pi k/\lambda$  is the absorption coefficient (where  $k$  is an imaginary part of the refractive index of

silicon), and  $L$  is the thickness of silicon. The reference curve (solid green line referred to as the Lambertian limit) in Fig. 11, for “ $4n^2$  light trapping” is obtained by inserting the experimentally measured values of  $\alpha$  for crystalline silicon. Using Eq. (3) and substituting it into Eq. (2), we obtain  $J = 31.2 \text{ mA/cm}^2$  for the Lambertian limit in the spectral range of 400–1100 nm and equivalent bulk thickness of silicon  $L = 1 \mu\text{m}$ .

The arguments leading to Eq. (5) for statistical light trapping were originally intended for conventional slabs where the light absorbing region is typically much thicker than the average wavelength.<sup>36</sup> For nano-photonic films with thicknesses comparable to or smaller than the wavelength, the ray-optics picture and many of the key assumptions in the statistical ray trapping picture are no longer applicable and the Lambertian limit can in principle be surpassed.<sup>40</sup> In Fig. 11, we show how the absorption calculated for the case of air cones exceeds the Lambertian limit over a broad spectral range of 300–1100 nm resulting in a 10% enhancement relative to the MAPD calculated using Eq. (5).

The MAPD of  $J = 34.2 \text{ mA/cm}^2$  achieved for the structure with a perfect conductor backreflector and no  $\text{SiO}_2$  packaging shown in the inset of Fig. 11 for the spectral range of 400–1100 nm is very close to the short circuit current ( $J = 34.6 \text{ mA/cm}^2$ ) obtained using twice the amount of silicon by Wang *et al.*<sup>51</sup> These authors consider a more complicated structure based on double-sided design where the top and bottom surfaces of a silicon slab are textured with cones with an equivalent bulk thickness of  $2 \mu\text{m}$  as well as a perfect back-reflector. The fabrication of this two-sided nano-structure involves more technological steps than our photonic crystal that can be generated using nano-imprint lithography techniques.<sup>50</sup> They also consider the broader spectral range of 300–1100 nm. Our structure using half the amount of silicon yields the MAPD of  $J = 35.5 \text{ mA/cm}^2$  in the extended spectral range of 300–1100 nm. In real solar cells, however, the near ultraviolet spectral range of 300–400 nm may not be accessible when the silicon is encapsulated and packaged with  $\text{SiO}_2$ .

## V. ANGULAR RESPONSE OF MAPD

A vital aspect of solar cell performance is the ability to absorb sunlight at off-normal incidence for both polarizations, over a wide angular range. In Fig. 12, we present the angular distribution of the MAPD for the unit cell geometry depicted in the inset with a perfect conducting backreflector and  $\text{SiO}_2$  packaging for the spectral range of 400–1100 nm. For each incidence angle  $\theta$  and each polarization channel, it is assumed that the entire AM 1.5 solar spectrum is collimated in that specific angle and channel. Fig. 12 demonstrates that no substantial degradation in the MAPD occurs at least up to  $\theta = 50^\circ$  for various directions of incidence. Both polarization channels yield strong off-normal MAPD characteristics, with p-polarization exceeding s-polarization MAPD for angles of more than  $20^\circ$  from normal incidence. Also in Fig. 12, we provide a comparison for the angular response between slanted cones and vertical cones. Clearly,

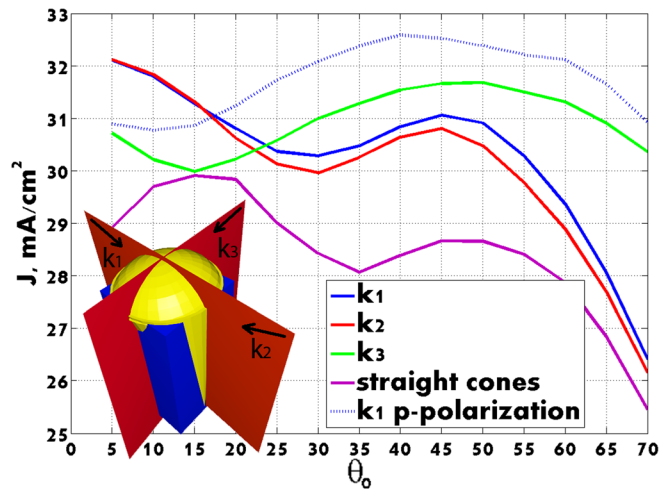


FIG. 12. Angular response of solar cell with a geometry shown on the inset with a perfect conducting backreflector and SiO<sub>2</sub> packaging for the spectral range of 400–1100 nm. All geometrical parameters are given in Fig. 9. Vectors  $k_1$  and  $k_2$  indicate directions of the incident wave in the plane of cone inclination and the vector  $k_3$  corresponds to the wave incidence in a plane perpendicular to the plane of cone inclination.

the slanted cone nano-pore geometry is preferable to vertical cones over a broad angular range.

## VI. CONCLUSION

In conclusion, we have demonstrated the efficacy of a silicon photonic crystal solar cell architecture with combined anti-reflection and light trapping properties. Our structure exhibits remarkable resonances in a spectral range of 800–1100 nm where light trapping occurs through a combination of energy flow parallel to the air-silicon interface and strong Poynting vector circulation in certain high intensity hot spots. This circulation enhances the dwell time of light in the thin-film over and above previously described parallel-to-interface refraction effects.<sup>34,38</sup> With only 1  $\mu\text{m}$  equivalent bulk thickness of silicon, our structure yields a MAPD of  $J = 35.5 \text{ mA/cm}^2$  over the spectral range of 300–1100 nm, prior to packaging in SiO<sub>2</sub>. With the addition of SiO<sub>2</sub> packaging, this MAPD drops to  $32.6 \text{ mA/cm}^2$  in the spectral range of 400–1100 nm. Both of these values are in excess of the so-called Lambertian ( $4n^2$ ) statistical ray trapping benchmark. In the spectral range from 800 to 1100 nm, we find a 25% increase in optical absorption relative to the  $4n^2$  benchmark. When the perfect conductor is replaced by a realistic silver back-reflector, the MAPD of the fully packaged structure drops from  $32.6 \text{ mA/cm}^2$  to  $32.3 \text{ mA/cm}^2$  in the spectral range of 400–1100 nm. We also calculated the variation of the MAPD with the angle of incidence of sunlight. Excellent solar absorption was found over a broad angular range of  $0^\circ$ – $50^\circ$ . Our results provide a graphic illustration that thin film photonic crystal can absorb more light than anticipated by conventional statistical ray trapping arguments. This occurs due to the enhancement in the effective path length of light due to the scattering within the photonic crystal microstructure and by a modification of the internal probability distribution of light flow directions, from that of a Lambertian distribution.

Unlike previously studied modulated nanowire photonic crystals<sup>34</sup> that were relatively insensitive to the inclusion of a metallic back-reflector, the absorption characteristics of our nano-pore PC is substantially improved by using a back-reflector. This leads to the MAPD that is roughly 20% better than is possible with an optimized nano-wire array.

The power conversion efficiency of our design is obtained by solving both Maxwell's and the semiconductor drift diffusion equations.<sup>35</sup> This takes into account the effect of the large surface area of our photonic crystal and the consequences of non-radiative recombination of carriers.<sup>35</sup> Using optimal junction and contact positions and including bulk and surface recombination losses, we find (using standard Si-SiO<sub>2</sub> surface and metal contact recombination velocities), solar power conversion efficiencies of at least 17.5% can be obtained for a carrier diffusion length of just a few microns.<sup>53–55</sup> This is an improvement compared to the 15% efficiency reported in optimized nanowire arrays with 1  $\mu\text{m}$  of silicon.<sup>35</sup>

This efficiency can be greatly improved if recombination at the metal contacts is reduced to the level found at our extensive Si-SiO<sub>2</sub> interface. Moreover, the very strong light intensities provided by our light trapping mechanism may be ideal for nonlinear upconversion of light at energies below the electronic band gap of silicon. Our numerical results suggest that there is a substantial opportunity for further efficiency enhancement of nanostructured solar cells. In future work we are planning to optimize power conversion efficiency of our conical pore photonic crystal solar cell. For this purpose, we are going to combine Electromagnetic Template Library,<sup>42</sup> used in presented here optical simulations, and Microvolt software for 3D semiconductor device modeling.<sup>56</sup> These two software packages are designed to support coupled electromagnetic and electrical modeling of solar cells.

## ACKNOWLEDGMENTS

This work was supported in part by the United States Department of Energy under Contract No. DE-FG02-10ER46754, the Natural Sciences and Engineering Research Council, and the Canadian Institute for Advanced Research.

<sup>1</sup>J. Grandier, D. M. Callahan, J. N. Munday, and H. A. Atwater, "Light absorption enhancement in thin film solar cells using whispering gallery modes in dielectric nanospheres," *Adv. Mater.* **23**, 1272–1276 (2011).

<sup>2</sup>J. Gjessing *et al.*, "Comparison of periodic light-trapping structures in thin crystalline silicon solar cells," *J. Appl. Phys.* **110**, 033104 (2011).

<sup>3</sup>F.-J. Haug *et al.*, "Resonances and absorption enhancement in thin film silicon solar cells with periodic interface texture," *J. Appl. Phys.* **109**, 084516 (2011).

<sup>4</sup>E. Garnett and P. Yang, "Light trapping in silicon nanowire solar cells," *Nano Lett.* **10**(3), 1082–1087 (2010).

<sup>5</sup>Z. Yu, A. Raman, and S. Fan, "Fundamental limit of light trapping in grating structures," *Opt. Express* **18**, A366–A380 (2010).

<sup>6</sup>A. Deinega, I. Valuev, B. Potapkin, and Yu. Lozovik, "Minimizing light reflection from dielectric textured surfaces," *JOSA A* **28**, 770–777 (2011).

<sup>7</sup>J. N. Munday and H. A. Atwater, "Large integrated absorption enhancement in plasmonic solar cells by combining metallic gratings and antireflection coatings," *Nano Lett.* **11**, 2195–2201 (2011).

<sup>8</sup>C. G. Bernhard, "Structural and functional adaptation in a visual system," *Endeavour* **26**, 79–84 (1967).

- <sup>9</sup>P. B. Clapham and M. C. Hutley, "Reduction of lens reflection by the 'Moth Eye' principle," *Nature* **244**, 281–282 (1973).
- <sup>10</sup>W. H. Southwell, "Pyramid-array surface-relief structures producing anti-reflection index matching on optical surfaces," *J. Opt. Soc. Am. A* **8**, 549–553 (1991).
- <sup>11</sup>D. H. Raguin and G. M. Morris, "Analysis of antireflection-structured surfaces with continuous one-dimensional surface profiles," *Appl. Opt.* **32**, 2582–2598 (1993).
- <sup>12</sup>B. L. Soporì and R. A. Pryor, "Design of antireflection coatings for textured silicon solar cells," *Sol. Cells* **8**, 249–261 (1983).
- <sup>13</sup>O. Bucci and G. Franceschetti, "Scattering from wedge-tapered absorbers," *IEEE Trans. Antennas Propag.* **19**, 96–104 (1971).
- <sup>14</sup>Y.-C. Chen and T.-M. Chen, "Improvement of conversion efficiency of silicon solar cells using up-conversion molybdate  $\text{La}_2\text{Mo}_2\text{O}_9\text{:Yb,R}$  (R = Er, Ho) phosphors," *J. Rare Earths* **29**(8), 723 (2011).
- <sup>15</sup>F. Sgrignuoli *et al.*, "Modeling of silicon nanocrystals based down-shifter for enhanced silicon solar cell performance," *J. Appl. Phys.* **111**, 034303 (2012).
- <sup>16</sup>Z. R. Abrams, A. Niv, and X. Zhang, "Solar energy enhancement using down-converting particles: A rigorous approach," *J. Appl. Phys.* **109**, 114905 (2011).
- <sup>17</sup>S. John, "Electromagnetic absorption in a disordered medium near a photon mobility edge," *Phys. Rev. Lett.* **53**, 2169–2173 (1984).
- <sup>18</sup>E. Yablonovitch, "Inhibited spontaneous emission in solid-state physics and electronics," *Phys. Rev. Lett.* **58**, 2059–2062 (1987).
- <sup>19</sup>S. John, "Strong localization of photons in certain disordered dielectric superlattices," *Phys. Rev. Lett.* **58**, 2486–2489 (1987).
- <sup>20</sup>K. Inoue and K. Ohtaka, *Photonic Crystals: Physics, Fabrication, and Applications* (Springer, Berlin, 2004).
- <sup>21</sup>M. Green, *Third Generation Photovoltaics* (Springer, Berlin, 2006).
- <sup>22</sup>*Nanotechnology for Photovoltaics*, edited by L. Tsakalacos (CRC Press, 2010).
- <sup>23</sup>G. Lozano, S. Colodrero, O. Caulier, M. E. Calvo, and H. Miguez, "Theoretical analysis of the performance of one-dimensional photonic crystal-based dye-sensitized solar cells," *J. Phys. Chem. C* **114**(8), 3681–3687 (2010).
- <sup>24</sup>P. Bermel *et al.*, "Improving thin-film crystalline silicon solar cell efficiencies with photonic crystals," *Opt. Express* **15**(25), 16986–17000 (2007).
- <sup>25</sup>P. G. O'Brien *et al.*, "Photonic crystal intermediate reflectors for micromorph solar cells: A comparative study," *Opt. Express* **18**(5), 4478–4490 (2010).
- <sup>26</sup>J. G. Mutitu *et al.*, "Thin film solar cell design based on photonic crystal and diffractive grating structures," *Opt. Express* **16**(19), 15238–15248 (2008).
- <sup>27</sup>J. Upping *et al.*, *Proc. SPIE* **7002**, 23 (2008).
- <sup>28</sup>T. Suezaki *et al.*, "Tailoring the electrical properties of inverse silicon opals—A step towards optically amplified silicon solar cells," *Adv. Mater.* **21**(5), 559–563 (2009).
- <sup>29</sup>Y. Song, J. Yu, and Y. Lee, "Antireflective submicrometer gratings on thin-film silicon solar cells for light-absorption enhancement," *Opt. Lett.* **35**(3), 276–278 (2010).
- <sup>30</sup>T. Stelzner, M. Pietsch, G. Andrea, F. Falk, E. Ose, and S. Christiansen, "Silicon nanowire-based solar cells," *Nanotechnology* **19**, 295203 (2008).
- <sup>31</sup>A. Kandala, T. Betti, and A. Fontcuberta, "General theoretical considerations on nanowire solar cell designs," *Phys. Status Solidi A* **206**, 173–178 (2009).
- <sup>32</sup>L. Tsakalacos, J. Balch, J. Fronheiser, B. A. Korevaar, O. Sulima, and J. Rand, "Silicon nanowire solar cells," *Appl. Phys. Lett.* **91**, 233117 (2007).
- <sup>33</sup>J.-Y. Jung *et al.*, "A strong antireflective solar cell prepared by tapering silicon nanowires," *Opt. Express* **18**(S3), A286–A292 (2010).
- <sup>34</sup>G. Demesy and S. John, "Solar energy trapping with modulated silicon nanowire photonic crystals," *J. Appl. Phys.* **112**, 074326 (2012).
- <sup>35</sup>A. Deinega and S. John, "Solar power conversion efficiency in modulated silicon nanowire photonic crystals," *J. Appl. Phys.* **112**, 074327 (2012).
- <sup>36</sup>E. Yablonovitch, "Statistical ray optics," *J. Opt. Soc. Am.* **72**(7), 899–907 (1982).
- <sup>37</sup>P. Campbell and M. A. Green, "Light trapping properties of pyramidally textured surfaces," *J. Appl. Phys.* **62**, 243–249 (1987).
- <sup>38</sup>A. Chutinan and S. John, "Light trapping and absorption optimization in certain thin-film photonic crystal architectures," *Phys. Rev. A* **78**, 023825 (2008).
- <sup>39</sup>D. Malacara and B. J. Thompson, *Handbook of Optical Engineering* (CRC Press, 2001), p. 684.
- <sup>40</sup>S. E. Han *et al.*, "Toward the Lambertian limit of light trapping in thin nanostructured silicon solar cells," *Nano Lett.* **10**, 4692 (2010).
- <sup>41</sup>A. Taflove and S. C. Hagness, *Computational Electrodynamics: The Finite-Difference Time-Domain Method*, 3rd ed. (Artech House Publishers, 2005).
- <sup>42</sup>See <http://fdtd.kintechlab.com> for Electromagnetic Template Library (EMTL), Kintech Lab Ltd.
- <sup>43</sup>See <http://rredc.nrel.gov/solar/spectra/am1.5/> for Reference Solar Spectral Irradiance: Air Mass 1.5.
- <sup>44</sup>A. Deinega and I. Valuev, "Subpixel smoothing for conductive and dispersive media in the FDTD method," *Opt. Lett.* **32**, 3429 (2007).
- <sup>45</sup>A. Deinega and I. Valuev, "Long-time behavior of PML absorbing boundaries for layered periodic structures," *Comput. Phys. Commun.* **182**, 149 (2011).
- <sup>46</sup>I. Valuev, A. Deinega, and S. Belousov, "Iterative technique for analysis of periodic structures at oblique incidence in the finite-difference time-domain method," *Opt. Lett.* **33**, 1491 (2008).
- <sup>47</sup>I. Valuev, A. Deinega, and S. Belousov, "Implementation of the iterative finite-difference time-domain technique for simulation of periodic structures at oblique incidence," *Comput. Phys. Commun.* (in press).
- <sup>48</sup>M. A. Green and M. Keevers, "Optical properties of intrinsic silicon at 300 K," *Prog. Photovoltaics* **3**, 189–192 (1995).
- <sup>49</sup>A. Deinega and S. John, "Effective optical response of silicon to sunlight in the finite-difference time-domain method," *Opt. Lett.* **37**, 112 (2012).
- <sup>50</sup>See <http://fdtd.kintechlab.com/en/fitting> for Fitting of dielectric function.
- <sup>51</sup>K. X. Wang, Z. Yu, V. Liu, Y. Cui, and S. Fan, "Absorption enhancement in ultrathin crystalline silicon solar cells with antireflection and light-trapping nanocone gratings," *Nano Lett.* **12**(3), 1616–1619 (2012).
- <sup>52</sup>T. Tiedje, E. Yablonovitch, G. D. Cody and B. G. Brooks, "Limiting efficiency of silicon solar cells," *IEEE Trans. Electron Devices* **ED-31**, 711–716 (1984).
- <sup>53</sup>Z. Yu, A. Raman, and S. Fan, "Fundamental limit of nanophotonic light trapping in solar cells," *Proc. Natl. Acad. Sci. U.S.A.* **107**, 17491–17496 (2010).
- <sup>54</sup>S. Y. Chou, C. Keimel, and J. Gu, "Ultrafast and direct imprint of nanostructures in silicon," *Nature* **417**(6891), 835–837 (2002).
- <sup>55</sup>A. Deinega, S. Eyderman, and S. John, "Coupled optical and electrical modeling of solar cell based on conical pore silicon photonic crystals," *J. Appl. Phys.* (to be published).
- <sup>56</sup>See <https://sites.physics.utoronto.ca/sajeevjohn/software/microvolt> for Microvolt, software for semiconductor devices modeling.